

Optical Wire Position Sensor

Patrick Bestmann, Andreas Herty, Friedrich Lackner
CERN, Geneva, Switzerland

Abstract

In the context of the Compact Linear Collider (CLIC) studies, a wire position sensor (WPS) is developed by Open Source Instruments Inc. This sensor is designed in order to be tested for its eligibility in the alignment concept based on a stretched wire system.

1 Introduction

The Compact Linear Collider (CLIC) studies at CERN are the plans for a future linear collider. Alignment concepts have to be proposed in order to achieve the demanded tolerance of 10 μm over a sliding window of 200 m along the accelerator. The detailed concept is presented by Becker et al. (2003) in CLIC note 553 and by Mainaud Durand and Touz  (2006) at the International Workshop on Accelerator Alignment in 2006.

For the transverse prealignment of the machine, overlapping stretched wire systems are proposed. In order to use the system for vertical measurements, the vertical wire catenary will be modelled by using hydrostatic levelling systems. For wire detection different sensors are under investigation. Open Source Instruments Inc is developing in cooperation with the European Organization for Nuclear Research (CERN) a low cost, optical wire position sensor (oWPS).

2 Design parameters

The design of the oWPS has been specified with the following parameters, derived from the constraints of the CLIC alignment.

- ± 5 mm dynamic range in x and y axis
- 5 μm rms absolute accuracy and precision
- 2 μm rms relative accuracy and precision

The given parameters are also in accordance to the WPS of FOGALE nanotech (fWPS) (Fogale nanotech, 2007). The sensors - fWPS and oWPS - can therefore be compared to each other.

3 Sensor

The sensor contains two cameras taking pictures of the same section of a stretched wire from two different angles. The calibration of each camera allows determining for each image a plane that contains the centre line of the wire. By intersecting these two planes, the centre line itself can be calculated. This centre line represents the wire. The cameras are installed on the vertical part of the sensor structure. Electronics and flash array are also installed on the sensor base plate. The light source used to illuminate the wire is a infrared light-emitting diode (LED) array. A photo of the sensor and the intersecting line concept is shown in figure 1.

The sensor has a mechanical interface in order to be connected to a geodetic network. Therefore the sensor is equipped with a kinematic ball mounting interface. This allows the installation of the sensor on Brandeis CCD Angle Monitor (BCAM) base mounting (Hashemi, 2002-2008a). The installation

Table 1: oWPS parameters

parameter	unit	WPS1-A	WPS1-B
CCD aperture	mm	9	10
CCD pivot	mm	11.4	10.4
diameter aperture	µm	250 ± 50	200 ± 5
centering aperture	µm	±1000	±100
lens focal length	mm	9	9
focal point of lens to CCD	mm	11	11
flat of lens to CCD	mm	10	12
CCD width	mm	3.4	
CCD height	mm	2.4	
CCD pixel size	µm	10 x 10	
field of view	mrad	±150 x ±100	±160 x ±110
aperture height above end plate	mm	15	15
aperture to front of CCD mounting plate	mm	4	5

4 Measurements

In order to validate the sensor's parameters a series of tests is proposed. The following tests have been carried out with the WPS1-A generation measuring on vectran wire:

- full and dynamic range measurements
- linearity measurements
- stability measurements

With the results of these tests an improved design has been put in place in order to have reliable results of the µm measurements for the WPS1-B generation. In addition to the tests mentioned above, the following tests have been carried out:

- stability measurements on stainless steel pin
- repeatability of the measurements

By using a common calibrated bench with kinematic ball mountings for each of the sensors, the following tests can be carried out:

- stability of all sensors on the same wire
- absolute calibration check of the sensors

The test setup will be presented with the according tests.

4.1 Equipment

4.1.1 Wire

The validation of a WPS is strongly linked the wire used for the test. For current monitoring applications at CERN, a carbon peek wire is used. This is due to the fact, that capacitive sensors from FOGALE nanotech have to be operated with a conductive wire (Herty, 2009). The oWPS does not have this limitation and can in principle be used with all types of wires.

In parallel, CERN investigates into a vectran wire. Vectran is a liquid crystal polymer fibre that offers a few very interesting advantages for alignment purposes. Such as a higher impact and break resistance,

low creep effect and less linear weight leading to smaller sag. At the moment, this fibre is the most likely to be used for future applications together with the optical sensors. The disadvantage is clearly the fact that it is almost transparent to infrared (IR) light. The fibre itself has been tested before by Lackner (2009) and Bestmann et al. (2009). The sensor tests have been carried out with the vectran fibre unless quoted different.

In order to see, if a difference in the wire detection of the sensors can be seen, the following types of wire have been chosen:

- carbon-PES
- tungsten $\varnothing 0.25$ mm
- beryllium-copper $\varnothing 0.1$ mm
- vectran

A Stability measurement with all wires show, that they can be used for measurements with the oWPS. The beryllium-copper wire is too thin to be correctly detected by the sensor. This problem is linked to the sensor as the principle of the two edge detection fails as the edges cannot be separated from each other.

In conclusion, all tested wires are suitable for the oWPS. In future tests measurements of a fWPS and an oWPS on the same carbon wire are possible.

4.1.2 Measurement environment

To obtain reliable, stable measurements in the μm range the laboratory has to fulfil some requirements. Air conditioning to better than 1°C , regulated access conditions and the stable installation and control of the references are some key points.

Motorized Newport micrometer stages are used to displace the wire in X and Y position. The manufacturer claims μm precision, which has not been controlled so far. Also the fact that the reference object, the wire, is moved during the measurements and not the sensors is something that needs to be changed in future tests.

4.1.3 Edge detection

The reliable edge detection of the wire is strongly depending on an image with the following properties:

- homogeneously illuminated background
- no shining edges of the wire
- detection method of the wire

The background is made of a white paper, glued to the sensor's cover. This thin screen provides a sufficiently homogeneous background though the aluminium cover is shining through.

The images are 8-bit, greyscale images. Due to the fact that vectran is almost transparent to IR light, the acquired images are showing a few contrast for the wire as shown in the original image in figure 2 on the left side. The intensified and smoothed image, showed on the right side of figure 2 is showing acceptable contrast for the wire detection algorithm.

4.2 Tests

4.2.1 Threshold scan

A critical parameter for the wire detection is the threshold that is applied to the derivative image. The choice of the threshold parameter is a compromise between the width of the detected wire edge and the

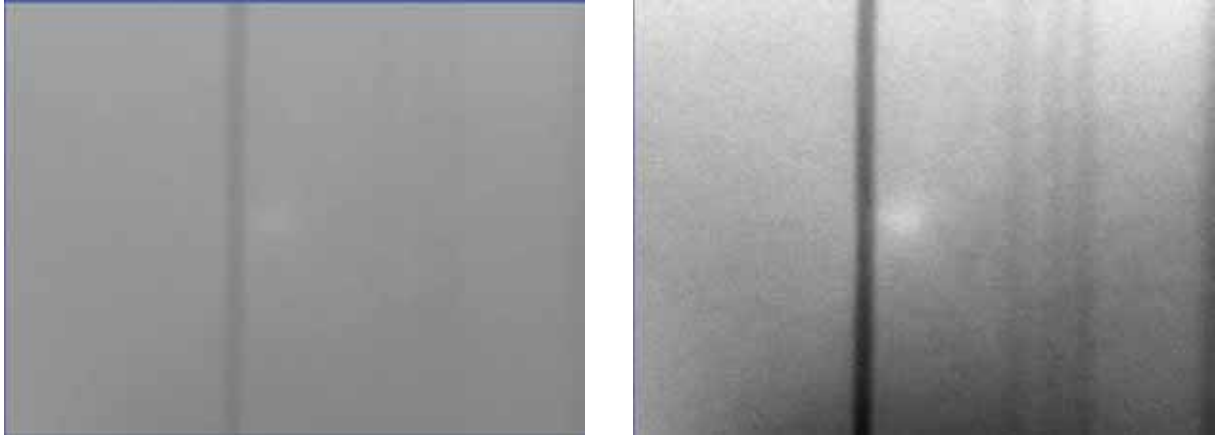


Fig. 2: Original (left) and intensified (right) 8-bit, greyscale image

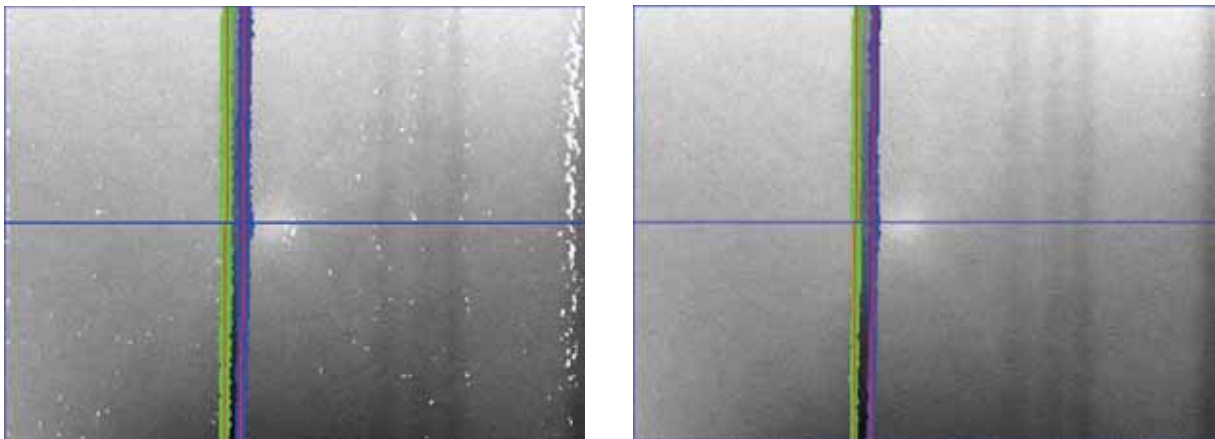


Fig. 3: edge detection with 10 percent (left) and 30 percent (right) threshold

width of the wire. The consequence of faulty parameters are, that in one extreme the detection of the edge is done only partially over the wire. This leads to a wrong determination of the wire position. The other extreme is, that the algorithm fails because the two edges cannot be separated anymore.

During tests the threshold value has been varied in order to find the best setting for the vectran wire. A threshold of 30 percent ($\text{analysis_threshold} = 30 \# 100$) from the average intensity to the maximum intensity has been used for all tests. This parameter setting provided the most stable results.

4.2.2 Stability on stainless steel pin

The stability measurement is based on the calibration concept of the sensor (Hashemi, 2008b). The calibration is carried out with respect to a stainless steel pin, that is displaced in the field of view of the sensor. As shown in figure 4, a pin support is glued to the sensor support plate for the stability test.

In order to avoid reflections on the shiny surface of the stainless steel pin, one pin has been blackened with a permanent marker and another pin has been mattfinished with sand paper. Best results were obtained with the blackened steel pin. This concept has been used for further tests.

Figure 5 shows the measurements of oWPS sensors P0199 and P0200 over four days pointing on blackened steel pins. P0199 has some outliers of about $3 \mu\text{m}$ in X and $1.5 \mu\text{m}$ in Y, where as the sensor

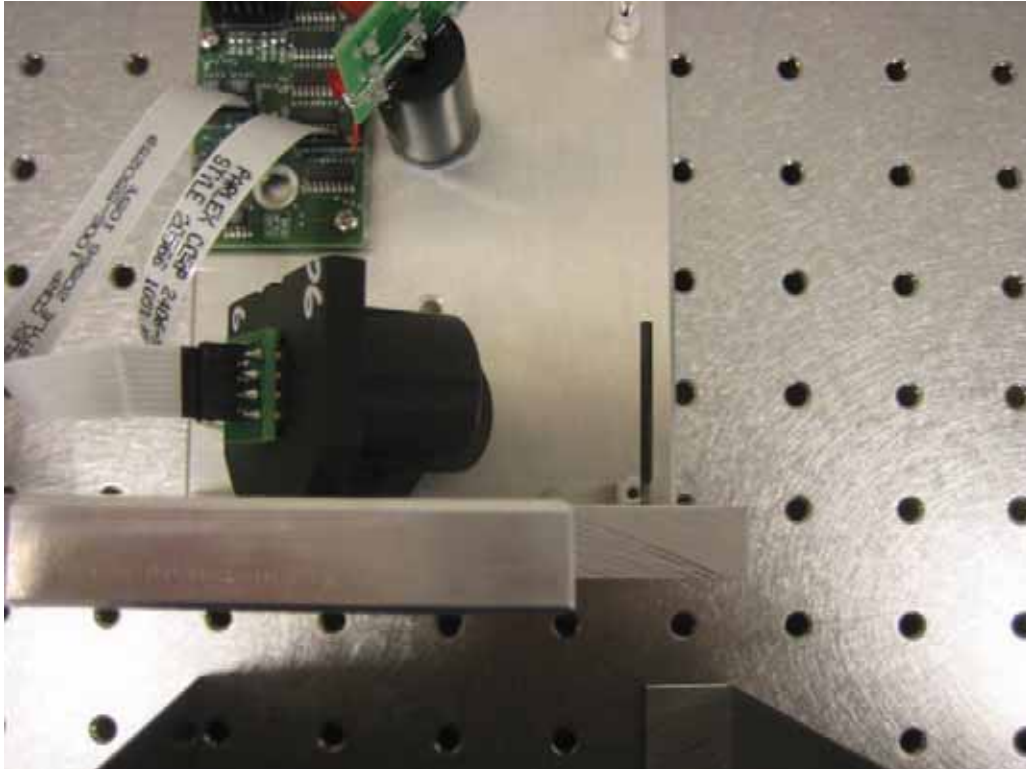


Fig. 4: stability measurement on pin

P0200 shows outliers only in the range of 1 μm on both axes.

The problem with these outlying measurements is, that they cannot clearly be identified, as they vary only by some micron from the true value. Statistical methods and averaging can help only together with a higher acquisition frequency.

4.2.3 *Stability on vectran*

Stability tests with the vectran wire are more delicate to provide a stable wire. The three sensor setup has been used to measure the stability of the sensors with the vectran wire in order to be able to determine a change in the reference wire. The analysis shows that this is not needed at the current state with the stability obtained. Figures 6 and 7 show the distribution of the deviations from the average value for the sensor P0200 in X and Y direction. There are four lines visible at distances of up to 7 μm from the average. This indicates that the main source of the problem is not linked to an unstable wire, but that difficulties in the detection of the vectran wire are the cause. The stability is about factor 7 worse using the vectran wire compared to a steel pin in a static setup (compare section 4.2.2).

In conclusion, all other tests carried out on a vectran wire and presented in this paper cannot be better than the 7 μm observed in this static setup.

4.2.4 *Range*

The test setup is based on four Newport micrometer stages which can be moved independently in vertical and horizontal direction. The stages are mounted perpendicular on two granite tables allowing the precise positioning of the wire inside the sensor's field of view at each extremity. The stages are equipped with linear encoders giving the stage position in sub- μm resolution in real-time. Figure 8 shows the layout of

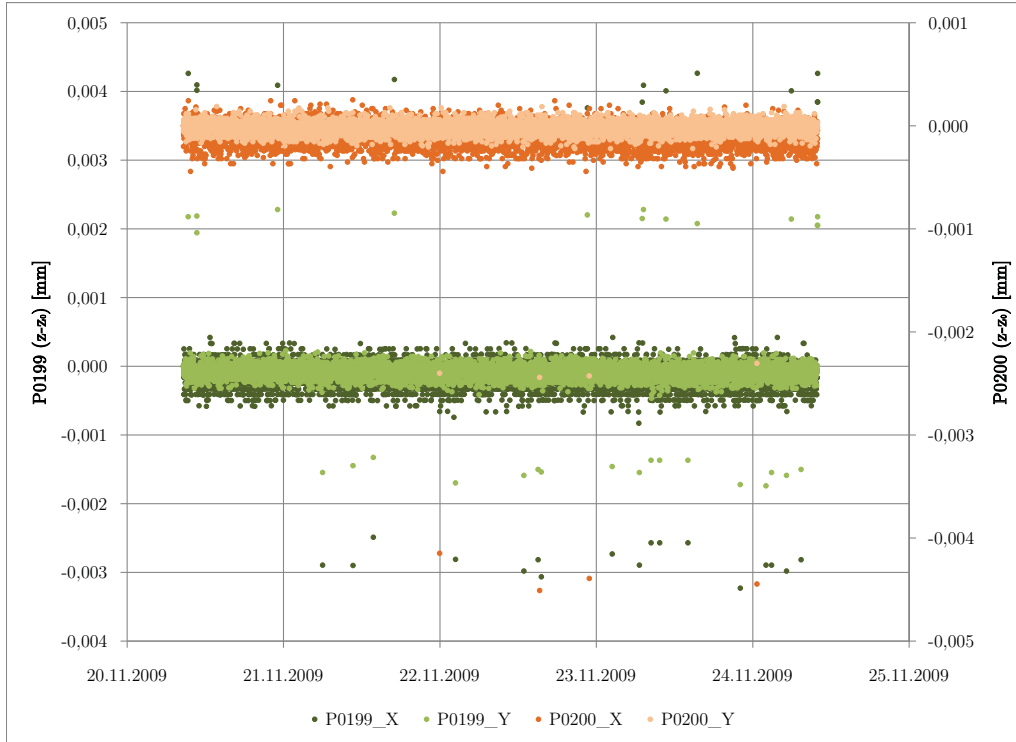


Fig. 5: stability measurement

the test setup.

The stages' specifications indicate $1.5 \mu\text{m} / 25 \text{ mm}$ and a bi-directional repeatability of $0.1 \mu\text{m}$ of the position accuracy.

The centre of the sensor is defined as $X_0 = 38 \text{ mm}$ and $Y_0 = 62.4 \text{ mm}$ following Hashemi's (2008b) drawing. The range measurement has been carried out by scanning an area from $X_{min} = 26 \text{ mm}$ to $X_{max} = 60 \text{ mm}$ in horizontal position and of $Y_{min} = 54 \text{ mm}$ to $Y_{max} = 74 \text{ mm}$ in vertical position in steps of 1 mm . The orange box in figure 9 is the specified dynamic range of $\pm 5 \text{ mm}$ around the centre point.

The specified range of $\pm 5 \text{ mm}$ in both axes was obtained, though limits can be seen in the corners. A diamond shaped field of view, as shown in figure 9, provides a measurement range of 280 mm^2 . The centre of the field of view varied for the sensor version WPS1-B by 2 mm in vertical direction. This brings the dynamic range of $\pm 5 \text{ mm}$ to the limits as far as the interchangeability is concerned.

4.2.5 Line of best fit

At the moment CERN does not have the possibility to control the absolute calibration of the sensors with μm precision. A calibrated test bench (Pugnat, 2009) with kinematic ball mounts for three sensors gives the possibility to compare the sensors with respect to each other. The sensors measure the same stretched wire at the same time. Following the calibration procedure, they deliver the position of the wire in the three ball mount systems. These coordinates are transformed into the test bench coordinate system that is known from the calibration. A straight line should be established from this calculation within the calibration tolerances of the bench that are $\pm 3 \mu\text{m}$.

The statistics of the deviation with respect to a straight line are shown in table 2. An rms of $4 \mu\text{m}$ in

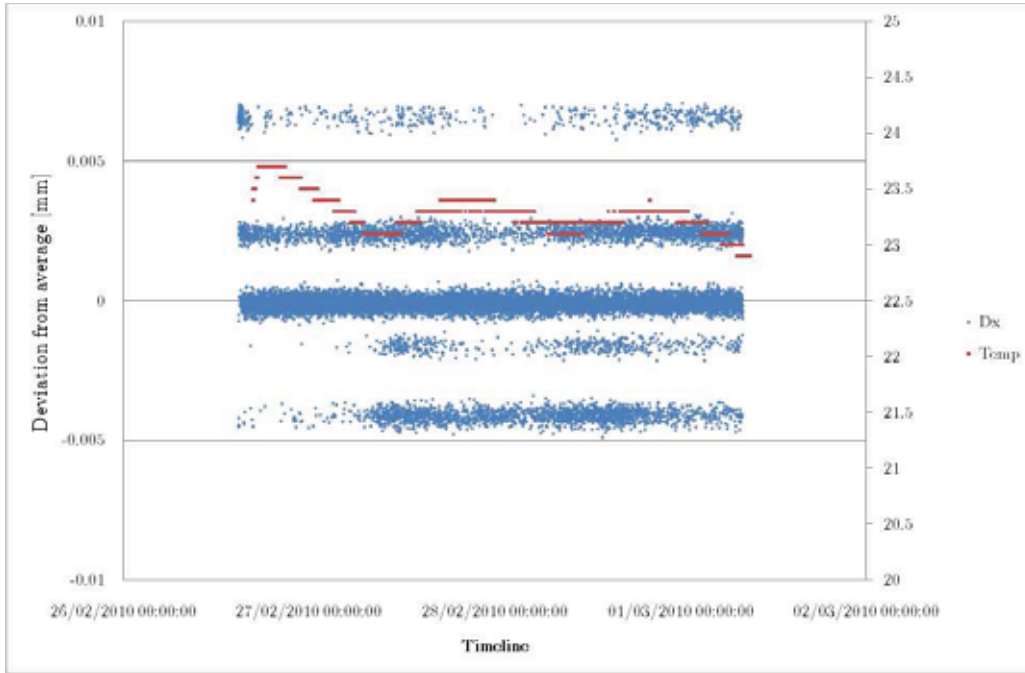


Fig. 6: stability measurement on vectran horizontal direction

vertical and $7 \mu\text{m}$ in horizontal direction is obtained. The factor of approximately 0.6 between the X and Y axis is due to the camera configuration. Details on this factor are given in section 4.2.6.

The deviations are plotted as vectors on the measured grid of 1 mm in figure 10. This test gives a clear image of the precision of these sensors as the sensors are checked against each other without any external effects to be taken into account. The disadvantage is that possible common and systematic effects of the sensors are also eliminated. The results become more optimistic in this case.

In this configuration one can see a deviation in the range of $35 \mu\text{m}$ in horizontal direction and $17 \mu\text{m}$ in vertical direction. The deviations of the dynamic range are normal distributed and centred for the vertical direction. They are slightly shifted by $5 \mu\text{m}$ to the positive side for the horizontal direction as shown in figures 11 and 12.

Taking the configuration and design parameters of the cameras with $10 \mu\text{m}$ by $10 \mu\text{m}$ pixel size and 11 mm focal length (compare table 1) the precision of the sensor can be evaluated as a function of the wire detection precision on the CCD. Assuming μm precision for the wire detection, one needs a resolution of 1/50 pixel for the detection of the wire on the CCD. Following (Hashemi, 2008b) the best resolution obtained with the vectran wire was $0.5 \mu\text{m}$, which corresponds to 1/20 pixel. This result was obtained with a three times thicker vectran wire and two times longer exposure time than used for this tests.

Calculated simulations based on a perfect, optical system and nominal parameters with $0.5 \mu\text{m}$ error in the wire edge detection are delivering results with a rms of $0.9 \mu\text{m}$ in horizontal and $0.5 \mu\text{m}$ in vertical direction. The spread is around $\pm 2.5 \mu\text{m}$ in horizontal and $\pm 1.5 \mu\text{m}$ in vertical direction.

The comparison between measurements and simulation leads to the conclusion that the sensor is not optimally configured for the vectran wire. Three possible causes have been identified, which can be the image resolution, the optics or the edge detection algorithm. From the mechanical point of view, the

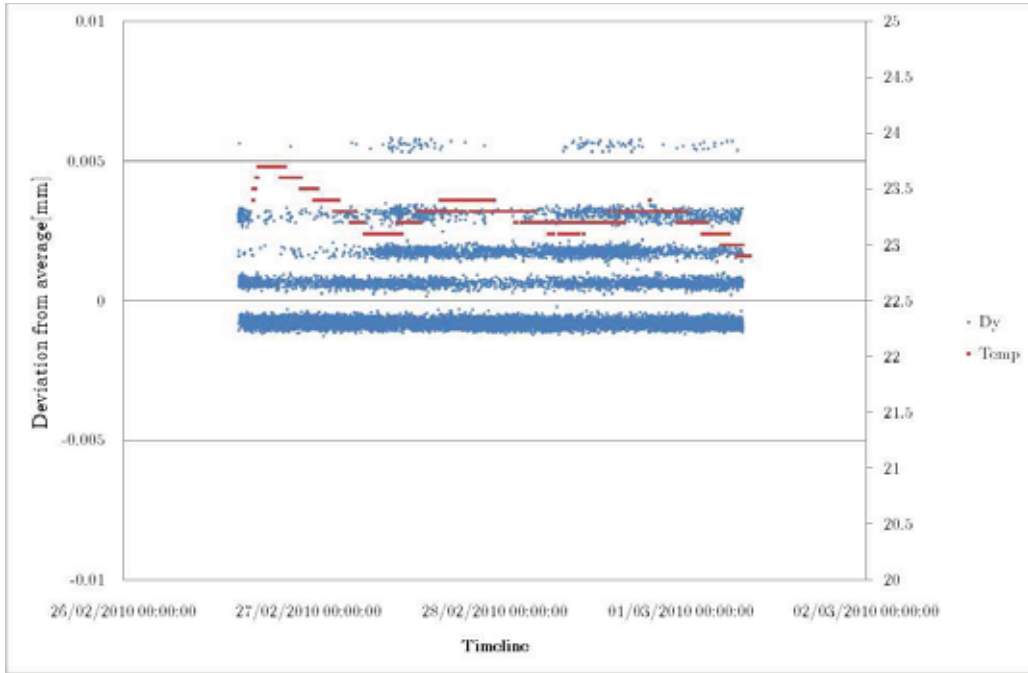


Fig. 7: stability measurement on vectran vertical direction

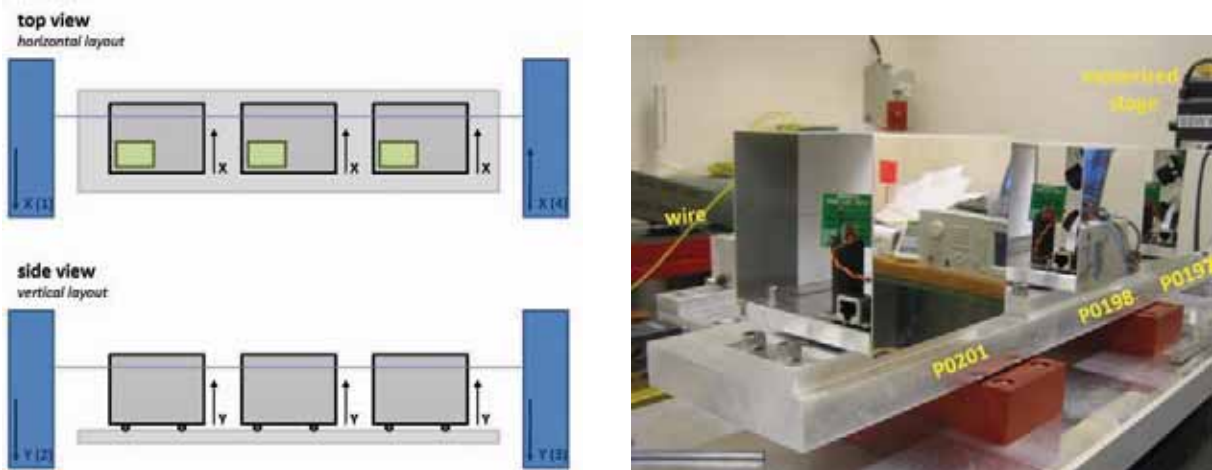


Fig. 8: test bench setup

camera configuration can also be revised in order to achieve the same precision in vertical and horizontal direction.

In addition to the difference between simulation and measurement, sensor P0195 has failed this line fit test, while being tested with P0202 and P0198. The deviations with respect to the straight line have been in horizontal direction approximately 400 μm . Changing the position of the sensor to the centre of the three sensor installation the offset was 890 μm in horizontal and 470 μm in the vertical direction. This leads to the conclusion that either the calibration of the sensor was wrong from the beginning or that the sensor was damaged during shipping to CERN.

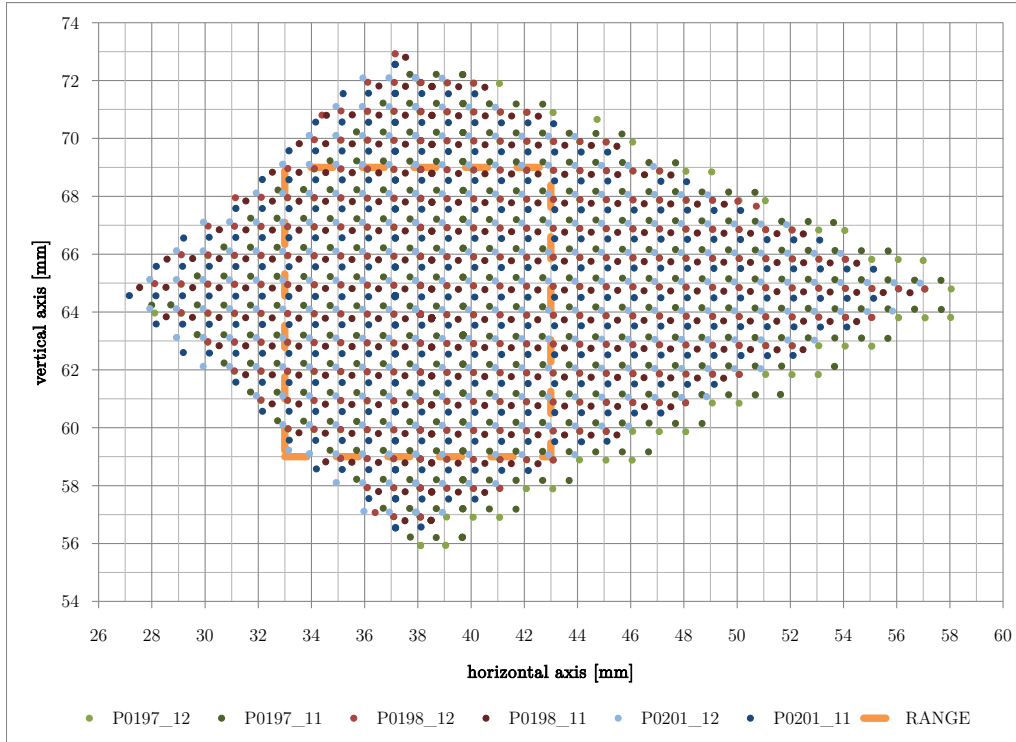


Fig. 9: oWPS range

Table 2: statistics for line fit deviations in the full range

parameter	dX	dY
min	-11.7	-10.1
max	30.8	13.3
range	42.5	23.4
average	5.4	0.8
rms	7.4	4.1

measurements in μm

Table 3: statistics for line fit deviations in the dynamic range

parameter	dX	dY
min	-11.7	-9.5
max	23.7	7.6
range	35.4	17.1
average	3.8	0.3
rms	6.1	3.2

measurements in μm

4.2.6 Repeatability

In order to test the repeatability of the oWPS, four identical measurements have been carried out. They were established as a line scan over the whole range of the sensor in distances of 1 mm. The four measurement cycles were compared with respect to each other. The obtained deviations can be plotted as vectors on the X and Y position plot in the regular 1 mm grid. Only the deviations are plotted regardless their position in the measurement field. A systematic effect is clearly visible at an angle of approximately 28° . Having in mind that the theoretical angle of the cameras is supposed to be 31° , this effect might

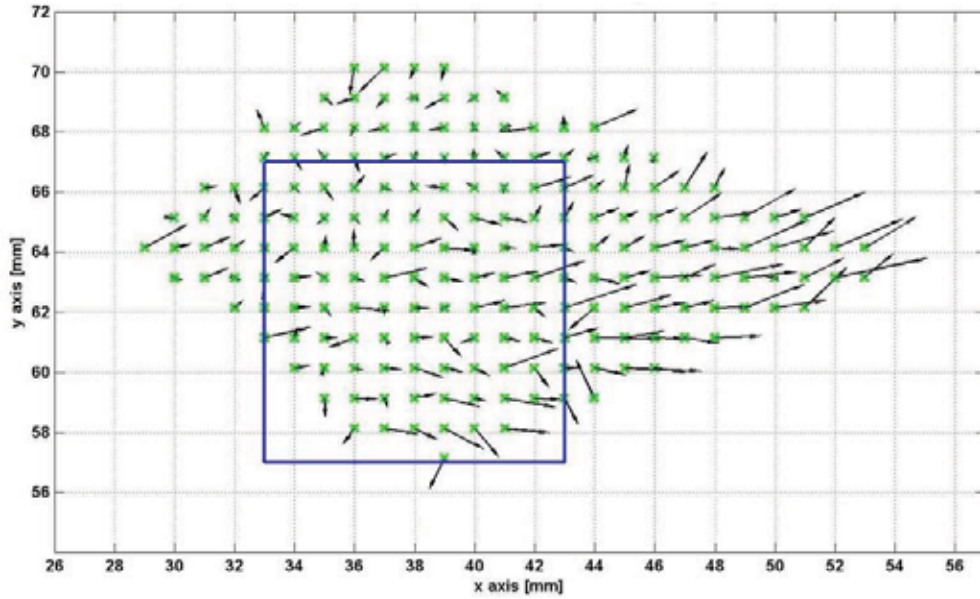


Fig. 10: oWPS line fit deviations

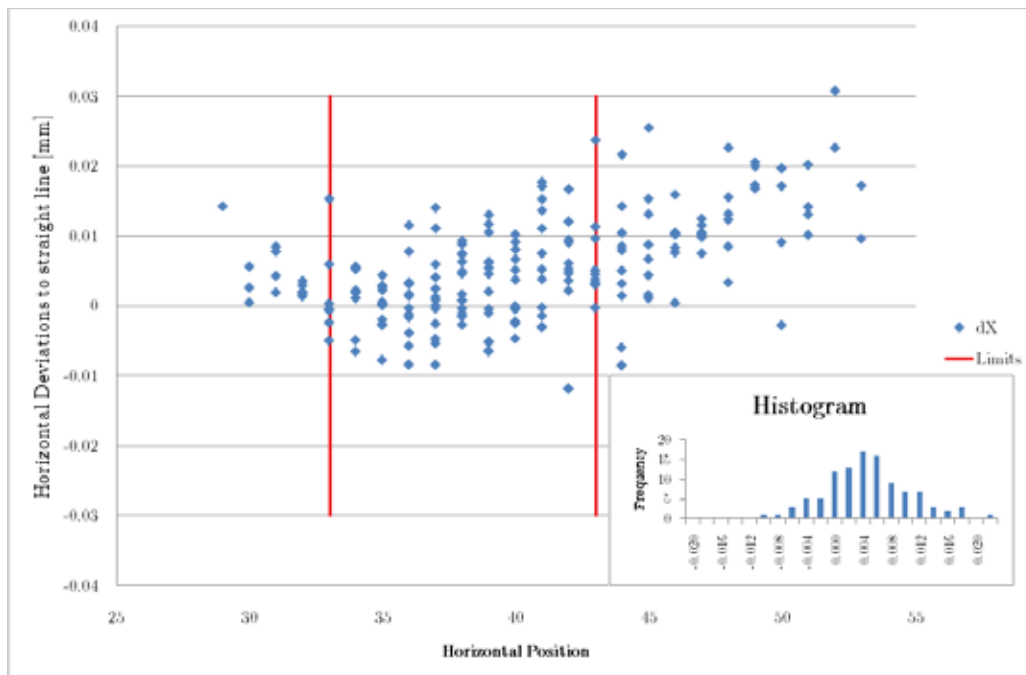


Fig. 11: oWPS line fit deviations X

linked to the camera configuration. The deviations are in the range of $\pm 5 \mu\text{m}$ in vertical and $\pm 10 \mu\text{m}$ in horizontal direction and therefore well in the range of stability measurements carried out on vectran wire in section 4.2.3. As the cameras are at 31° from the horizontal position, the horizontal direction is affected by the cosine and the vertical direction by the sine. Therefore the factor of $\tan 31^\circ = 0.6$ can be deduced as difference between horizontal and vertical accuracy.

This systematic effect is still visible when reducing the dataset to the 10 mm by 10 mm dynamic range in the centre of the sensor. In order to compare the measurements to the calibration of Open Source

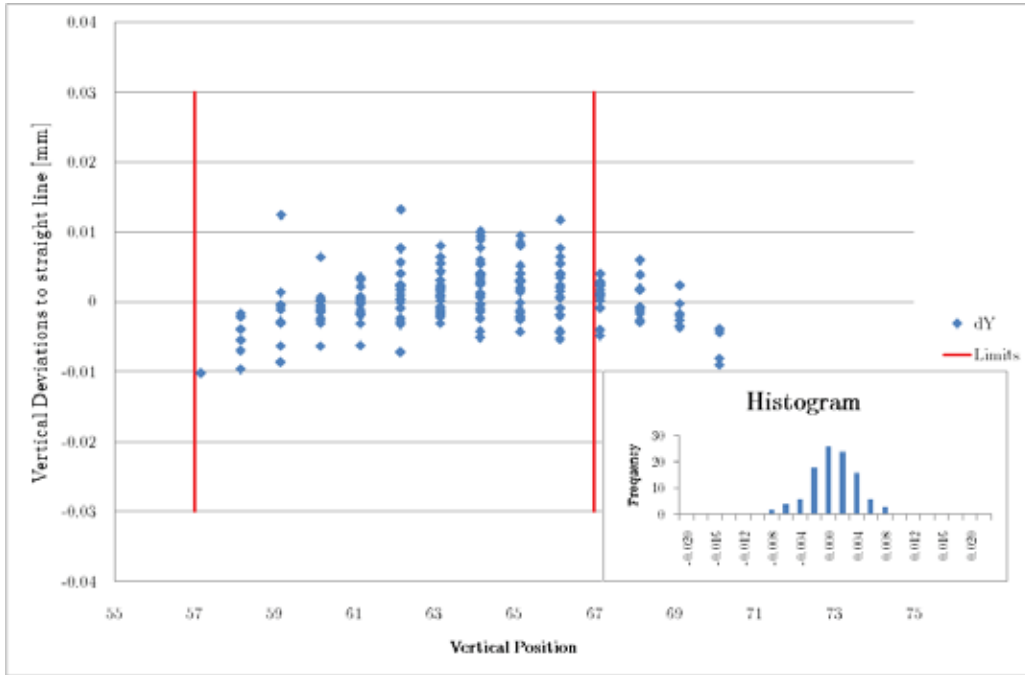


Fig. 12: oWPS line fit deviations Y

Instruments, the data set has been reduced to 14 positions that are used for the calibration. In this configuration, the systematic effect is no longer obvious. In addition, the points used for the calibration are mostly situated in the upper half of the measurement field. A possible explanation can be the precision of the edge detection in combination with the vectran wire. These random detection errors would again propagate with sine and cosine, creating an elliptical shape with the factor 0.6 on the main axes. This assumption is graphically evaluated in figure 13. As shown in the annex, the shape in these figures stays the same for all sensors and all differences. Also when reducing again the dataset to the 10 mm by 10 mm dynamic range, there is still a group of points forming a straight line at an angle of 28°.

4.2.7 Linearity

The linearity of the oWPS is tested with measurements that are comparing the displacements measured by the micrometer stages to the sensor's reading. Therefore the full range of the oWPS measurement field is scanned in steps of 1 mm. For a first analysis the resulting coordinates are reduced to the first measurement in the centre of the sensor and the oWPS displacements are subtracted from the stage displacements.

The obtained deviations can be plotted as vectors on the X and Y position plot in a regular 1 mm grid as shown in figure 14. In a raw data plot, the deviations seem to be important. This can though be explained as the coordinate axes of the stages are not necessarily corresponding to the X and Y axes of the oWPS. Orienting the direction of the three sensors and the stages is difficult and so the rotation between the axes is eliminated by a best fit transformation of the oWPS coordinate set on the coordinates of the stages. The residuals in X and Y direction can again be plotted on the 1 mm grid as shown in figure 15. The application of the best fit transformation does not change the statistic values shown in table 4.

In the case, that the dataset of the full range measurement is reduced to the dynamic range of 10 mm by 10 mm the rms is reduced by almost 50 percent as presented in table 5. The linearity test shows the same spread as the repeatability test. This means that the obtained deviations are random taken into

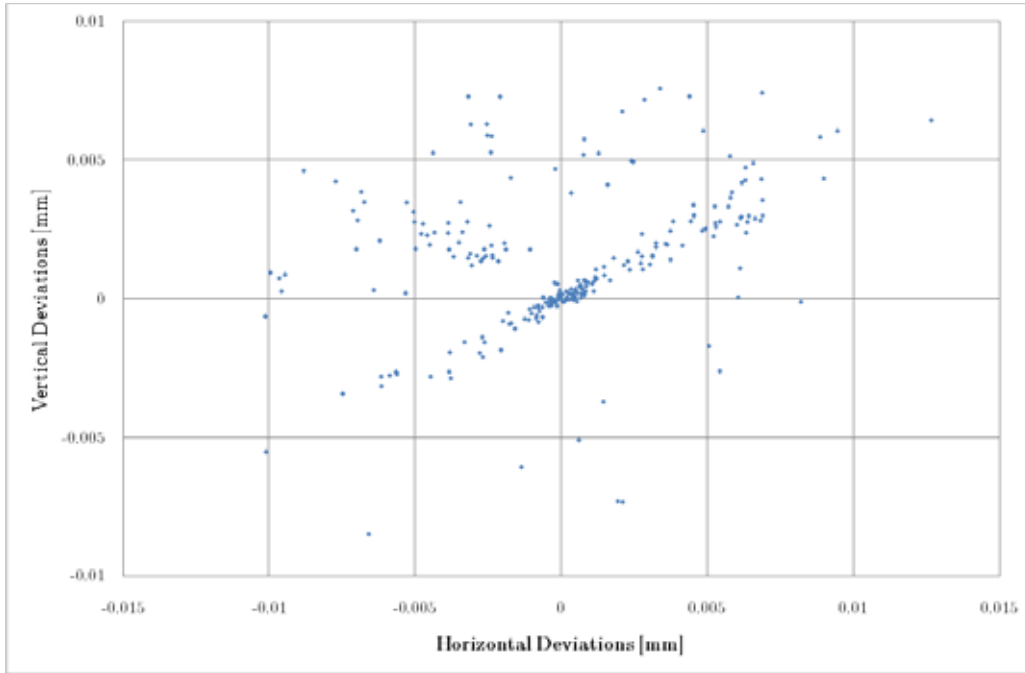


Fig. 13: oWPS repeatability XY deviations on full range

Table 4: statistics for linearity tests full range

	P0200		P0201		P0197	
	dX	dY	dX	dY	dX	dY
min	-37	-19	-55	-24	-66	-34
max	31	18	13	17	25	16
range	68	37	69	41	90	50
average	0	2	-3	0	-12	-1
rms	11	4	9	6	11	6

measurements in μm

account today's measurement configuration. A straight line, being a systematic effect, is still visible due to the sensor layout.

It can be concluded, that the sensor has a linear behaviour within the dynamic range. This can be shown as good as the limits of the setup and the sensor precision of 5 to 10 μm . This result can only be reduced by improving the test setup and in a second step improvement of the sensors as for example a modification of the wire fitting algorithm or the camera resolution with respect to the vectran wire.

4.3 Illumination

The influence of different illumination angles and types of illumination has been investigated. This test has been introduced as the calibration of the oWPS is carried out on a test stand with illumination from behind while the sensor is measuring on a steel pin (Hashemi, 2008b). In the measurement configuration, the illumination comes from a side position as shown in the sensor layout in figure 1. The difference in this configuration could lead to an offset in the measurement.

In a test setup with an IR array flashing from behind, as during calibration, and from the side, as during

Table 5: statistics for linearity tests dynamic range

	P0200		P0201		P0197	
	dX	dY	dX	dY	dX	dY
min	-14	-7	-13	-15	-25	-9
max	15	9	13	11	25	16
range	29	16	26	26	50	24
average	1	1	-2	1	-5	1
rms	5	3	5	4	7	3

measurements in μm

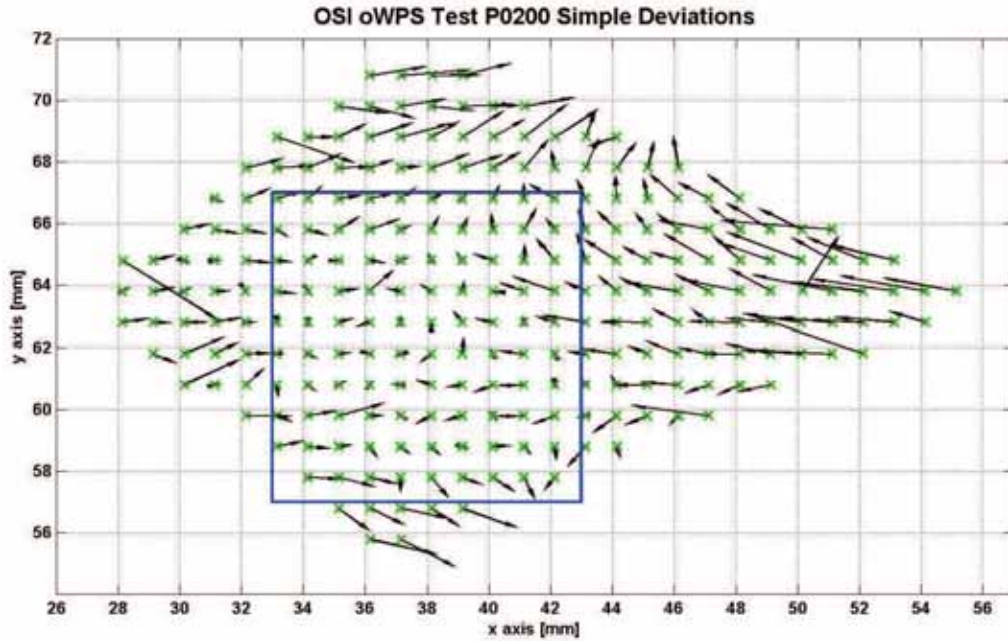


Fig. 14: scan with simple deviations (oWPS P0200)

normal operation, shows differences between these two measurement methods of approximately $10\ \mu\text{m}$ with a vectran wire.

In contrast to the calibration and standard configuration, the vectran wire is almost transparent for IR light. This results in a poor contrast for the wire on the images of the CCD cameras. The constraints of the vectran manufacturer are, that the wire cannot be produced in another colour and the only way to improve the results. A possible solution can on be to adapt the light source to the wire. Some tests using green LED illumination have shown promising as shown in figure 16. As the LED array is made of a different array, it has not been optimized to create a homogeneous background in the image.

5 Software

The software used for the data acquisition of the oWPS is provided by Open Source instruments under public license. though the code is available, the modification of the software is not evident, especially in the field of acquisition through the LWDAQ system, the fitting algorithm for the wire edge detection and the intersection of the lines.

Depending on the special application some data acquisition scripts have to be written in Tcl/Tk in collaboration with Open Source Instruments in order to acquire the measurements and analyse the results

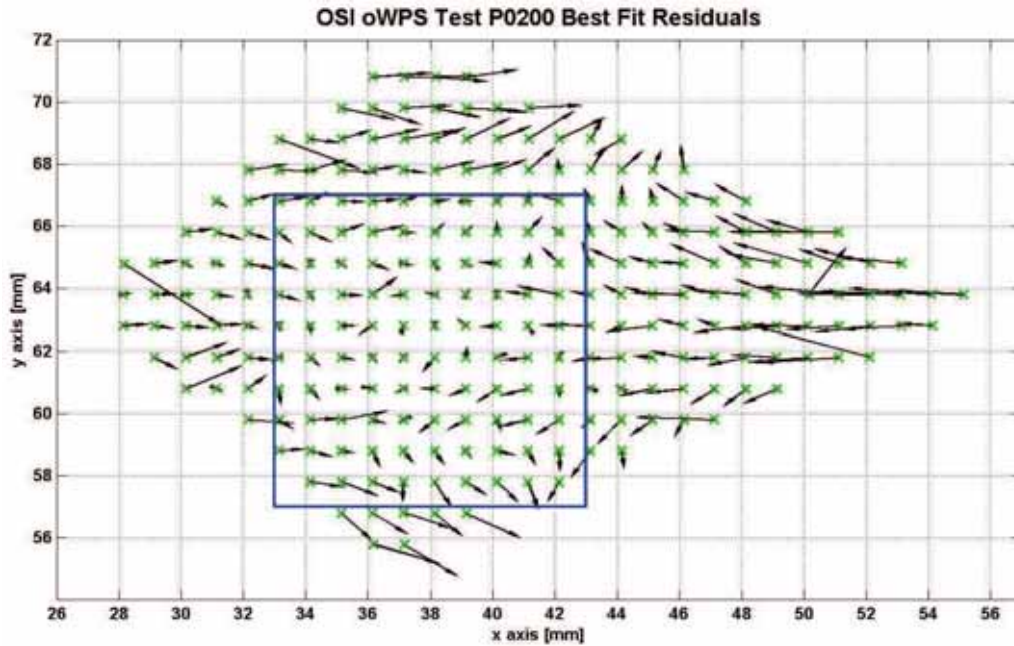


Fig. 15: scan with best fit residuals (oWPS P0200)

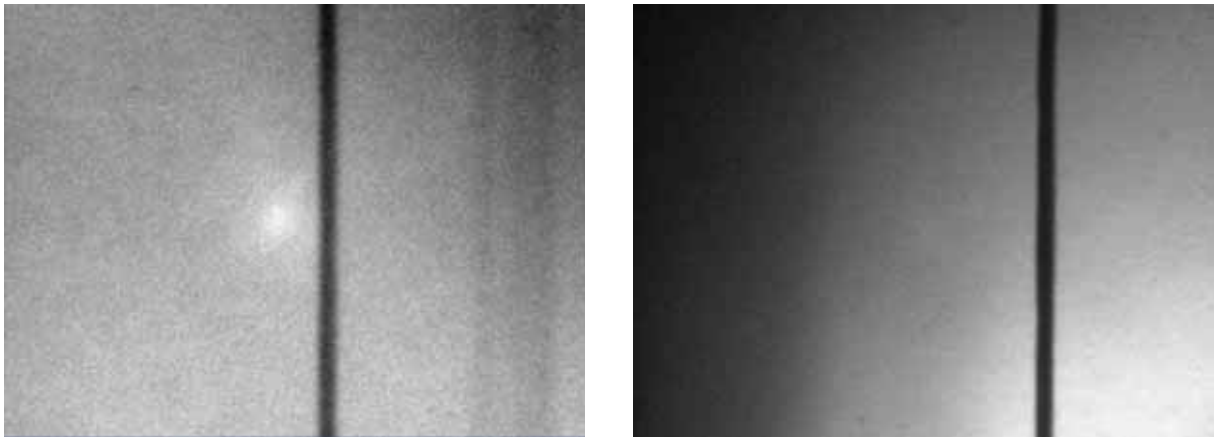


Fig. 16: intensified images for IR (left) and green LED (right) array

of several sensors at the same time.

Data acquisition software has been written at CERN in order to combine oWPS measurements together with the Newport stages and monitor a strain gauge as monitor for the wire tension. A screen shot of the software is presented in figure 17. The interfaces that are used are

- the stage driver that is connected using RS232 serial port connection
- the oWPS via TCP/IP to the data acquisition (DAQ) board
- the strain gauge voltage measurement using a Keithley DMM Scanner on a GPIB interface

The program reads a text file with the parameters for automatically driving the Newport stages. At each defined position, the actual position of the stages is measured followed by the strain gauge voltages and the oWPS coordinates set. All results are grouped in one single log file that can be used for further data analysis. The format of the file is the following presented in one single row as:

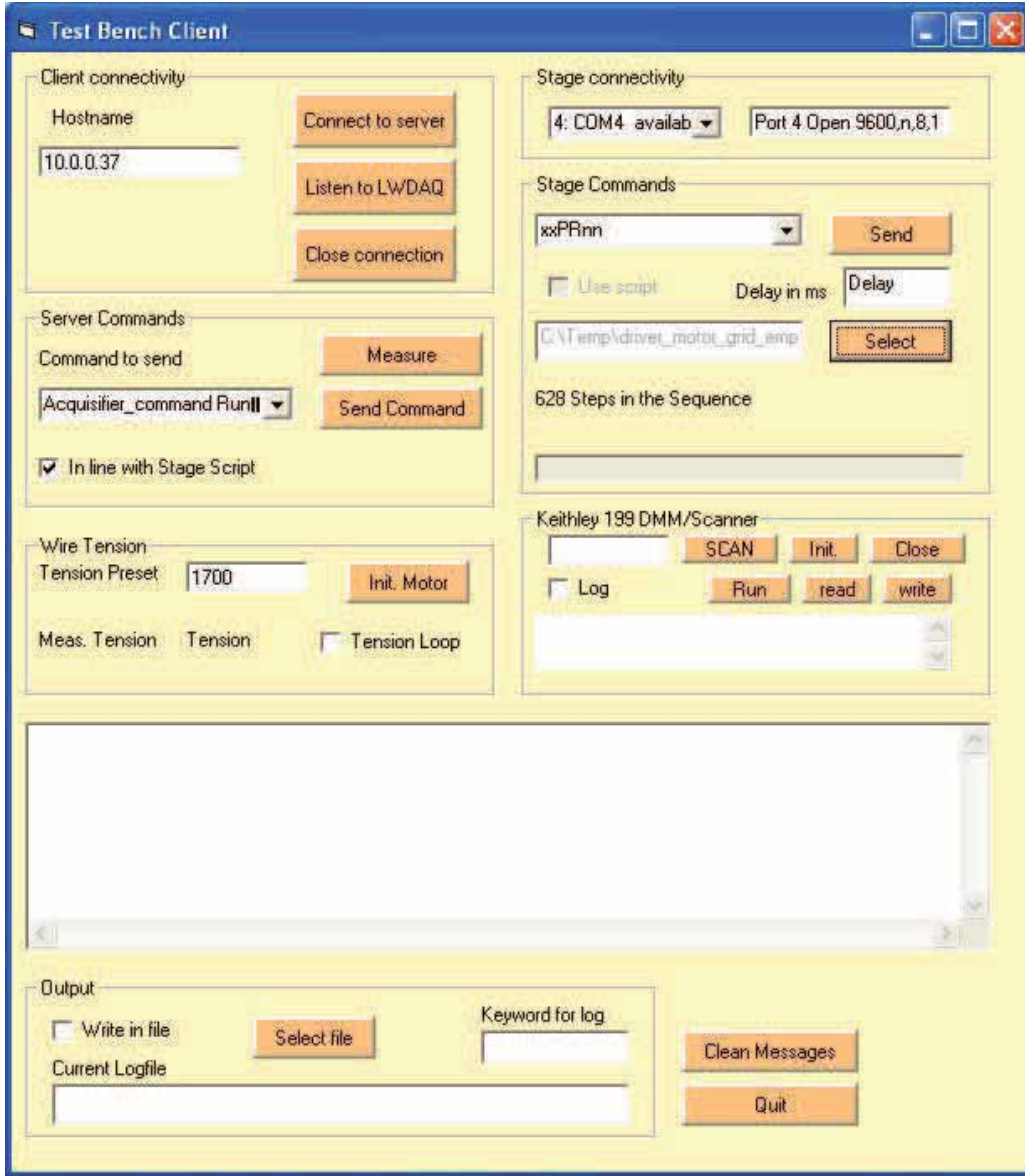


Fig. 17: screenshot of the client software

$\underbrace{\text{date; time; excitation voltage; signal voltage; P1; P2; P3; P4}}_{\text{date parameters}}$
 $\underbrace{\text{strength gauge}}_{\text{strength gauge}}$
 $\underbrace{\text{stage positions}}_{\text{stage positions}}$
 $\underbrace{\text{oWPS time; S1X; S1Y; S1Z; S2X; S2Y; S2Z; S3X; S3Y; S3Z;}}_{\text{stage positions}}$
 $\underbrace{\text{oWPS \#1}}_{\text{oWPS \#1}}$
 $\underbrace{\text{oWPS \#2}}_{\text{oWPS \#2}}$
 $\underbrace{\text{oWPS \#3}}_{\text{oWPS \#3}}$

The DAQ rate of sensors from Open Source Instruments is limited by the sequential readout of the sensors. The DAQ time, t_{oWPS} , for one oWPS reading is defined by the parameters shown in equation 1

$$t_{oWPS} = f_{C1} + f_{C2} + p + w \quad (1)$$

The parameter f is the flash time of each camera, $C1$ and $C2$. The processing time to calculate the wire position is defined with the parameter p and the time before the next sensor can be measured is w . All

parameters are given in seconds.

The flash time, f , is the limiting factor in the equation, as for the detection of the wire a time of approximately 0.2 s per camera is needed. The global estimation for one single measurement is $t_{oWPS} = 1$ s. This is independent from the sensor version.

6 Proposals

During these test ideas came in order to carry out further tests. In this section, tests are proposed in order to be able to get a better resolution of the measurements, design aspects of the sensor are discussed as well as analysis methods are proposed for a reliable wire detection.

6.1 Tests

The test benches for dynamic applications as range and linearity measurements have to be based on a concept, where the wire reference is kept in a static and stable position, where as the sensors are moved across their range. A three or more sensor setup shall be used in order to redundantly control the absolute calibration of the sensors.

While applying mechanical changes to the setup, the longitudinal force applied to the wire has to be controlled with suitable electronics. The given strain gauge was not suitable for the application and has therefore not been taken into account.

The use of IR light was optimized for measurements with a steel pin and corresponding to the sensitivity of the CCD array of the camera. Depending on the wire that is used for the application, in this case preferably vectran, the best light source has to be sorted out. Measurements with an array of green LEDs showed in first results, that the contrast is much better and that at the same time the exposure time is not longer. Other light sources and positions have to be tested for a final conclusion in this field.

6.2 Design aspects

The mechanical layout of the sensor can be optimized. Three aspects have been identified: the housing, the electronics and the size of the sensor. The size of the sensor can be minimized and better balanced by installing the electronics differently on the base plate. This allows at the same time a better protection of the electronics in case the wire breaks. The housing should be modified to be a fix part of the sensor.

The problem with monitoring sensors is often the redundancy of the measurement. This can be solved by adding a second sensor in the position to be measured. In the case of the oWPS, one can imagine installing a third camera that allows a second analysis of the wire position. This can also lead to an improvement in both measurement axes and eliminate the problem of a vertically better determined position.

6.3 Analysis methods

The wire used as reference has an length specific frequency in which it oscillates. The sequential image acquisition is therefore a problem, when coming to μm stability of the wire. The wire can in addition to its own frequency also have induced frequencies as for example due to ventilation or ground vibration.

The wire detection relies on a two edges detection. In the case of thin wires, this can lead to problems with the detection as seen for diameters of 0.25 mm and less. A gauss fit for each line to identify the centre of the wire should improve the measurements and provides at the same time a rms which can be used to evaluate the quality of each measurement.

The acquisition frequency is depending mostly on the exposure time and the serial acquisition as shown in section 5. The estimation shows, that measurements are at the moment possible for one single sensor at a frequency of 1 Hz. The frequency decreases with every additional sensor installed. The given configuration is too slow for an active alignment setup and no statistical means can be used to detect faulty measurement or a non-stable wire.

6.4 Calibration

The calibration is based on 22 measurements of 14 points as described by (Hashemi, 2008b). All points are situated in the upper half of the sensor's field of view. A homogeneous distribution in the full range of the sensor or in the dynamic range has to be foreseen. With an automated measurement more points can be measured in order to determine the calibration parameters. The interchangeability of the sensor is with the actual parameters only ensured to ± 1 mm as shown with the measurements.

A first approach, can be a recalculation of the existing calibration parameters with the measurements carried out during the range scan of the sensor - as presented in section 4.2.4.

7 Conclusion

The tests have shown that the oWPS are close to the design specifications. The available setup does not allow any investigation to better than 10 μm for dynamic measurements. Modifications in the bench concepts have to be established in order to be able to measure in the range of the demanded accuracy for CLIC applications.

The two sensor generations WPS1-A and WPS1-B show already modifications that allow better measurements in generation B. In the near future, a new generation is to be manufactured as the CCD chips are no longer available.

With the tests carried out on the sensors and the proposals for mechanical modifications, a more powerful generation can be established. This generation can come closer to the CLIC specifications, but in order to validate the performance, the test benches have to be reviewed.

Appendices

A Abbreviations

Abbreviation	Description
B	
BCAM	Brandeis CCD Angle Monitor
C	
CCD	Charge-coupled device
CERN	European Organization for Nuclear Research
CLIC	Compact Linear Collider
D	
DAQ	Data Acquisition
F	
fWPS	FOGALE nanotech WPS
I	
IR	infrared
L	
LED	Light-emitting diode
O	
oWPS	Open Source Instruments WPS
P	
PES	Polyethersulfone
R	
rms	root mean square
W	
WPS	Wire Position Sensor

References

- Becker, F., Coosemans, W., Pittin, R. and Wilson, I. H. (2003). *An Active Pre-Alignment System and Metrology Network for CLIC*, CERN, Switzerland, available at: <http://cdsweb.cern.ch/record/604004/files/open-2003-011.pdf>.
- Bestmann, P., Herty, A., Kershaw, R., Lackner, F. and Spevack, R. J. (2009). *Stretched Wire Test with Vectran Fibres*, CERN, Switzerland, available at: <https://edms.cern.ch/file/1016406/1/Report-Vectran-Test.docx>.
- Fogale nanotech (2007). *Etalonnage des capteurs HLS et WPS*, presentation, FOGALE nanotech, 125 rue de l'hostellerie, Bâtiment A, 30900 Nîmes, France, available at: https://edms.cern.ch/file/856493/1/etalonnage_wps_hls.pdf.

- Hashemi, K. (2002-2008a). *BCAM User Manual*, available at: http://alignment.hep.brandeis.edu/Devices/BCAM/User_Manual.html.
- Hashemi, K. (2008b). *WPSI Calibration*, available at: <http://www.opensourceinstruments.com/WPS/>.
- Herty, A. (2009). *Micron precision calibration methods for alignment sensors in particle accelerators*, available at: https://edms.cern.ch/file/1013828/1/2009-06-03_mphil_herty.pdf.
- Lackner, F. (2007). *Design and high precision monitoring of detector structures at CERN*, Technische Universität Wien. PhD thesis.
- Lackner, F. (2009). *Wire as a Reference for future Accelerators*, CERN, Switzerland, available at: <https://edms.cern.ch/file/997702/1/BE-ABP-SU-Lackner-Wire-Reference.pdf>.
- Mainaud Durand, H. and Touzé, T. (2006). *The Active Prealignment of the CLIC Components*, 9th International Workshop on Accelerator Alignment, SLAC, USA, available at: <http://www.slac.stanford.edu/econf/C06092511/papers/WE006.PDF>.
- Pugnat, D. (2009). *Plaque metrologique 9 spheres*, CERN, Switzerland, available at: <https://edms.cern.ch/file/1008996>.

Appendices

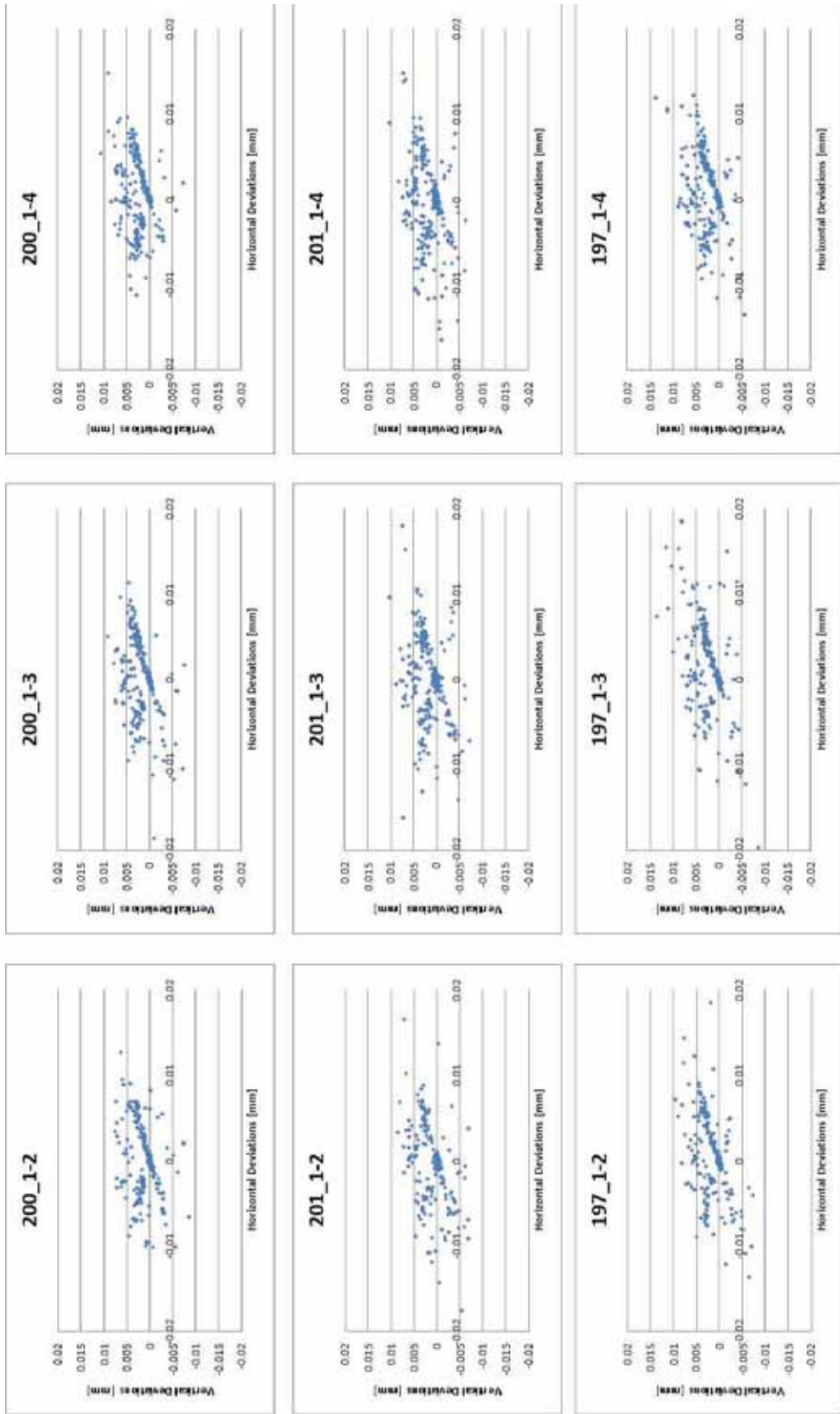


Fig. .1: oWPS repeatability test epoch differences 1

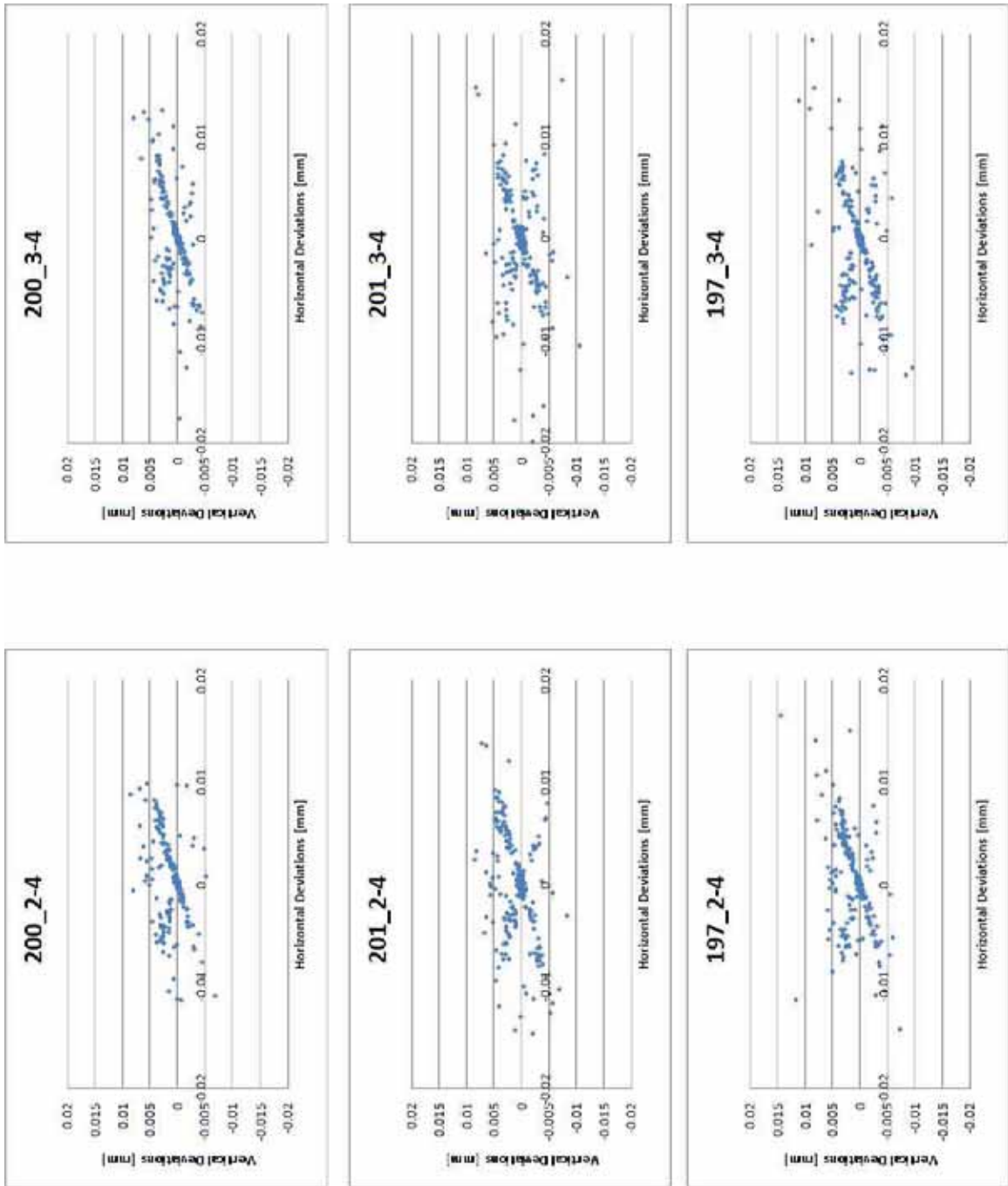
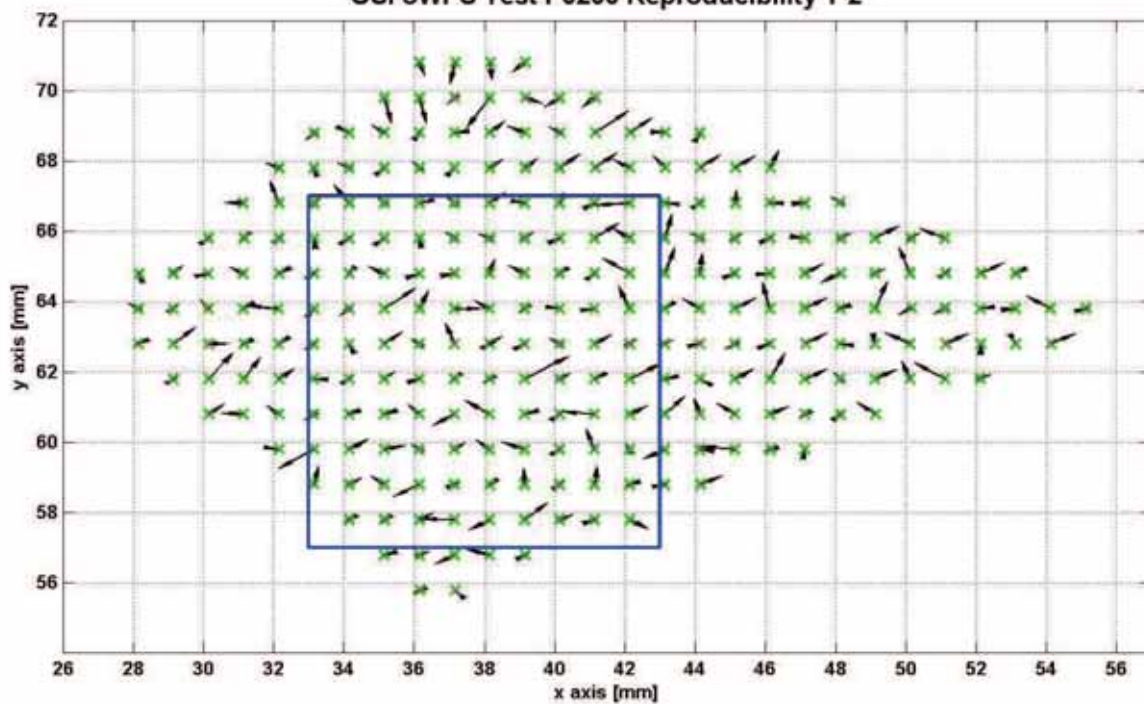
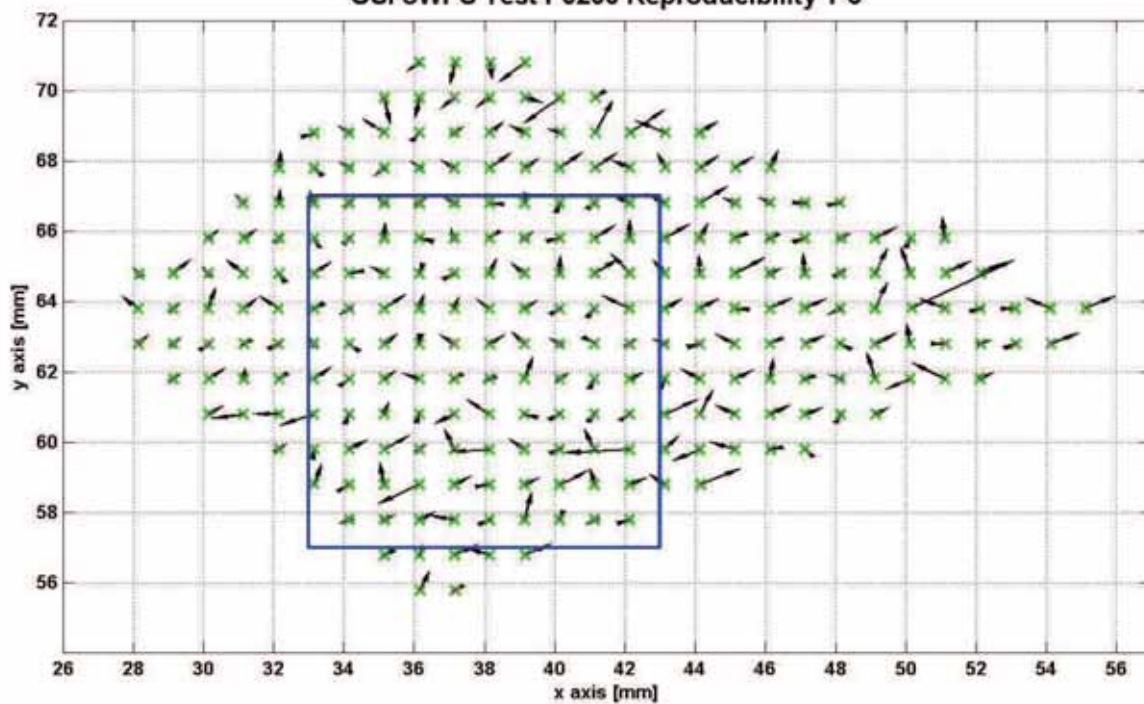


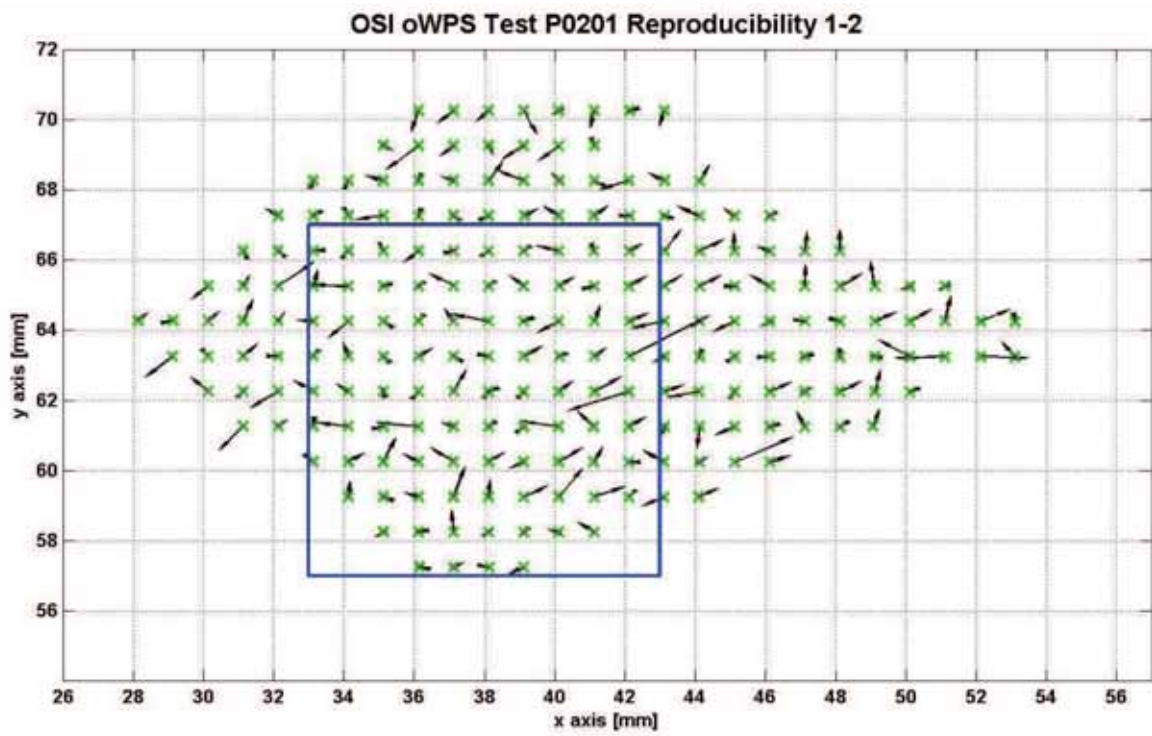
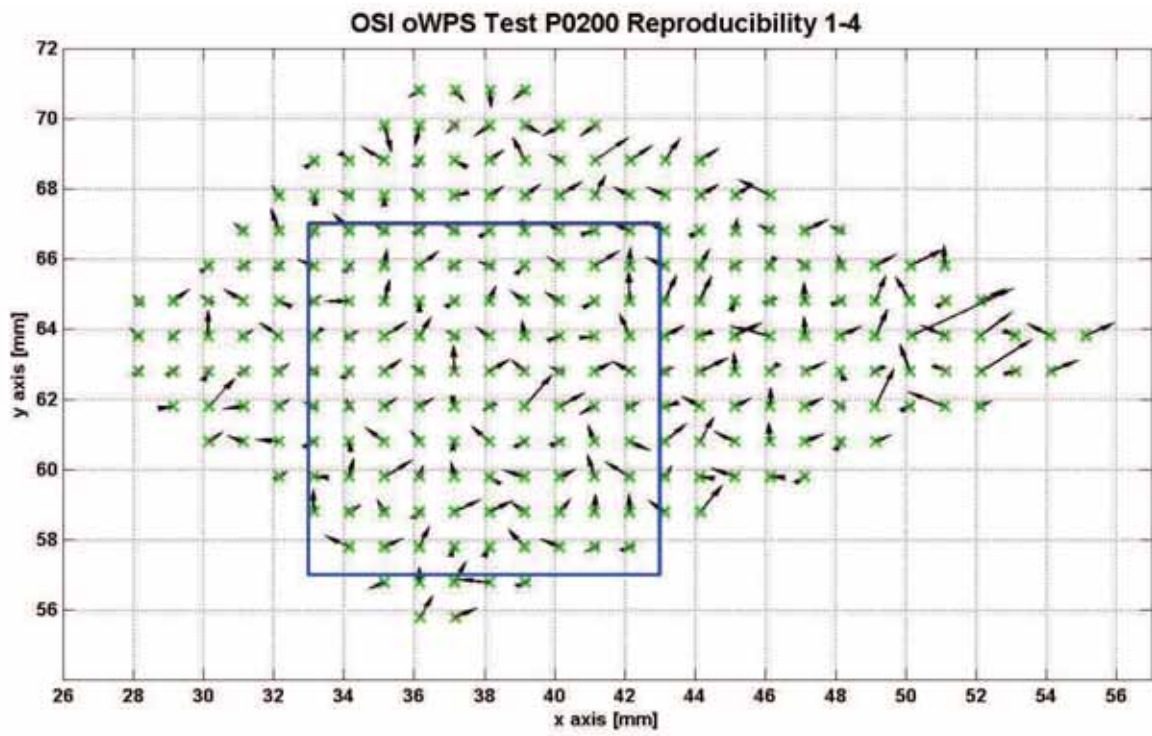
Fig. .2: oWPS repeatability test epoch differences 2

OSI oWPS Test P0200 Reproducibility 1-2

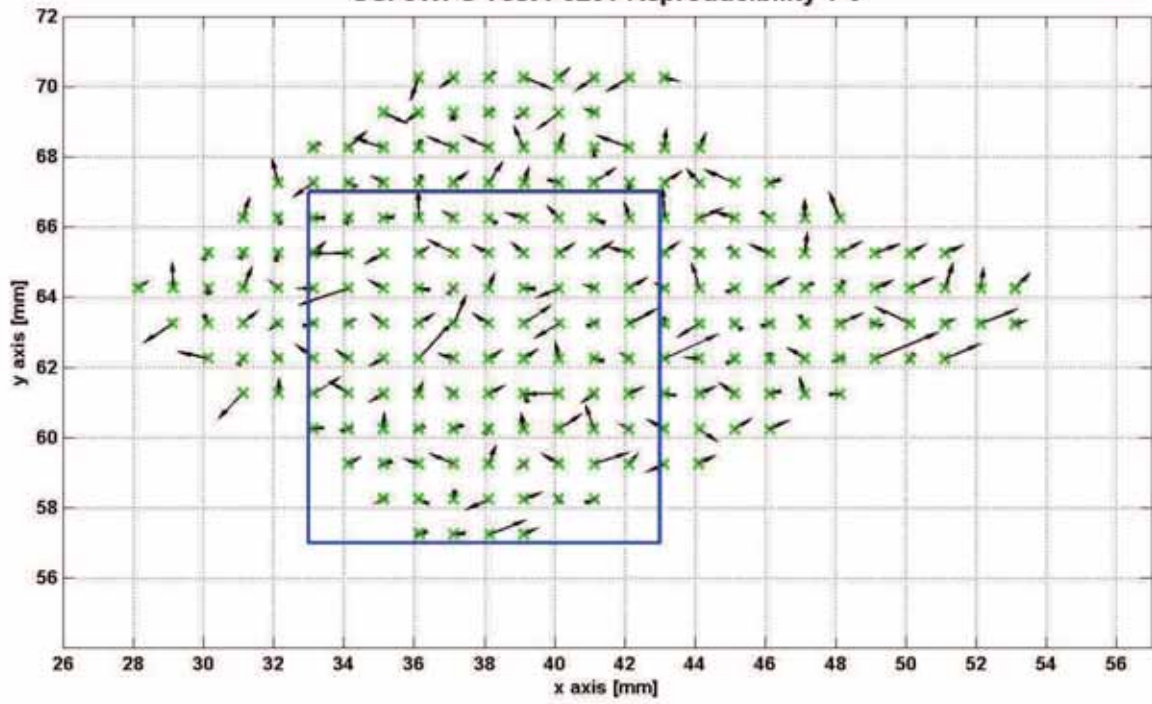


OSI oWPS Test P0200 Reproducibility 1-3

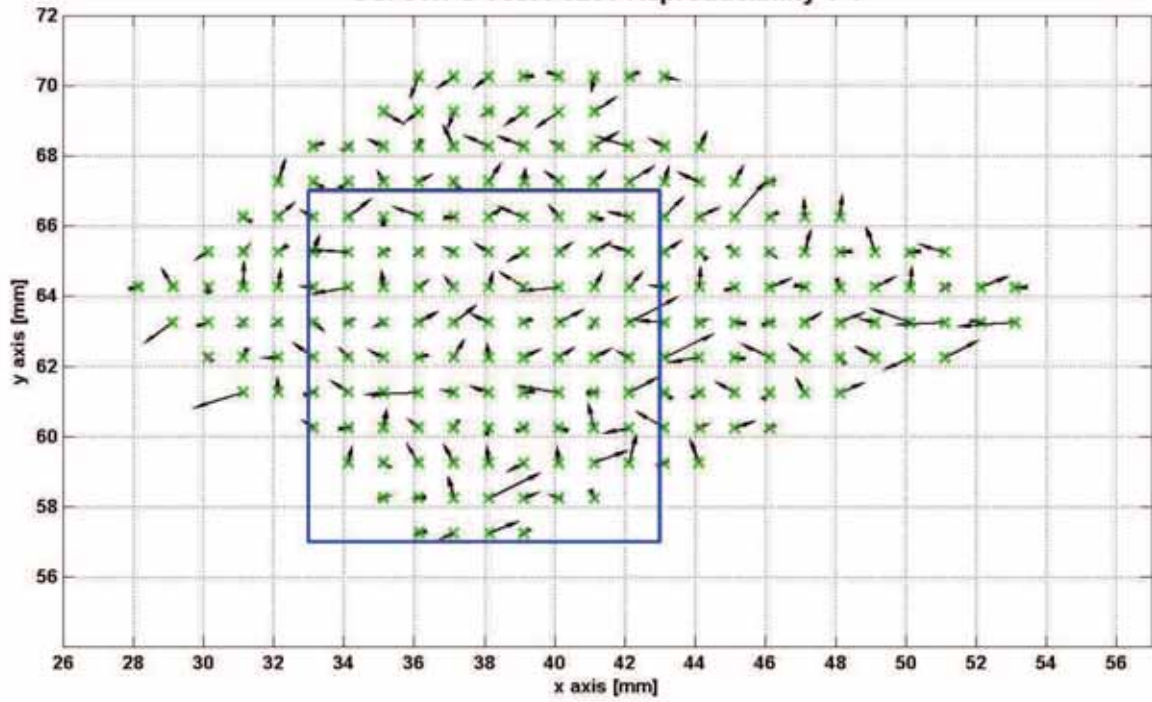




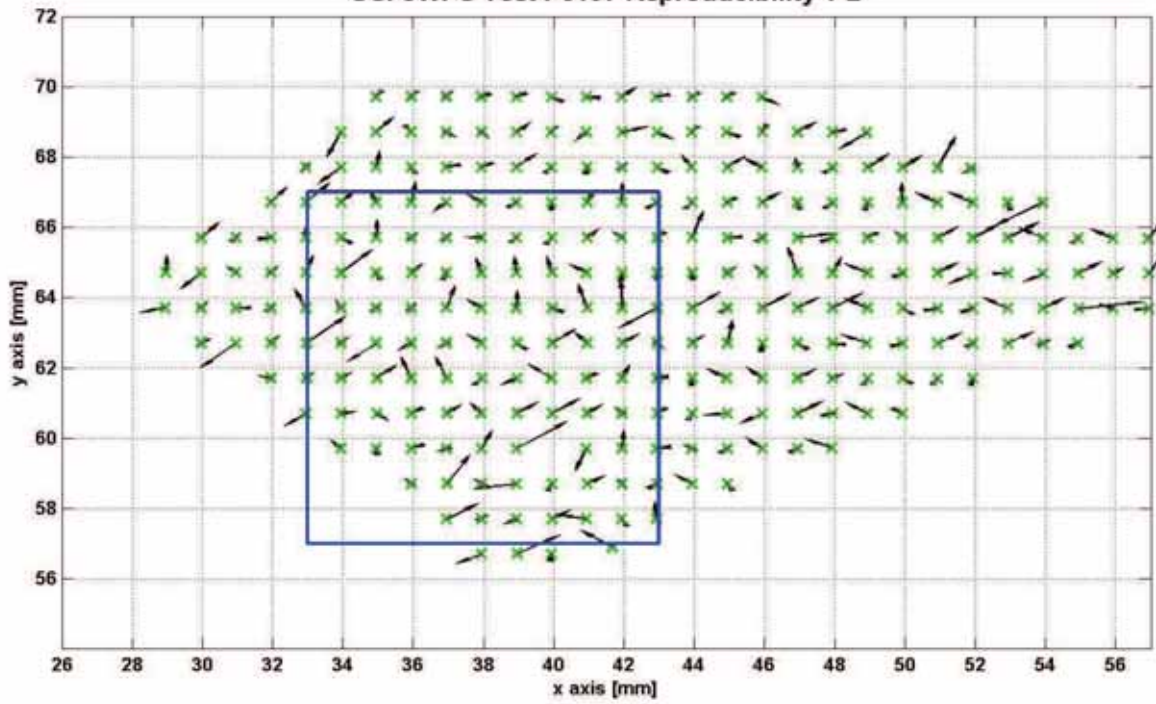
OSI oWPS Test P0201 Reproducibility 1-3



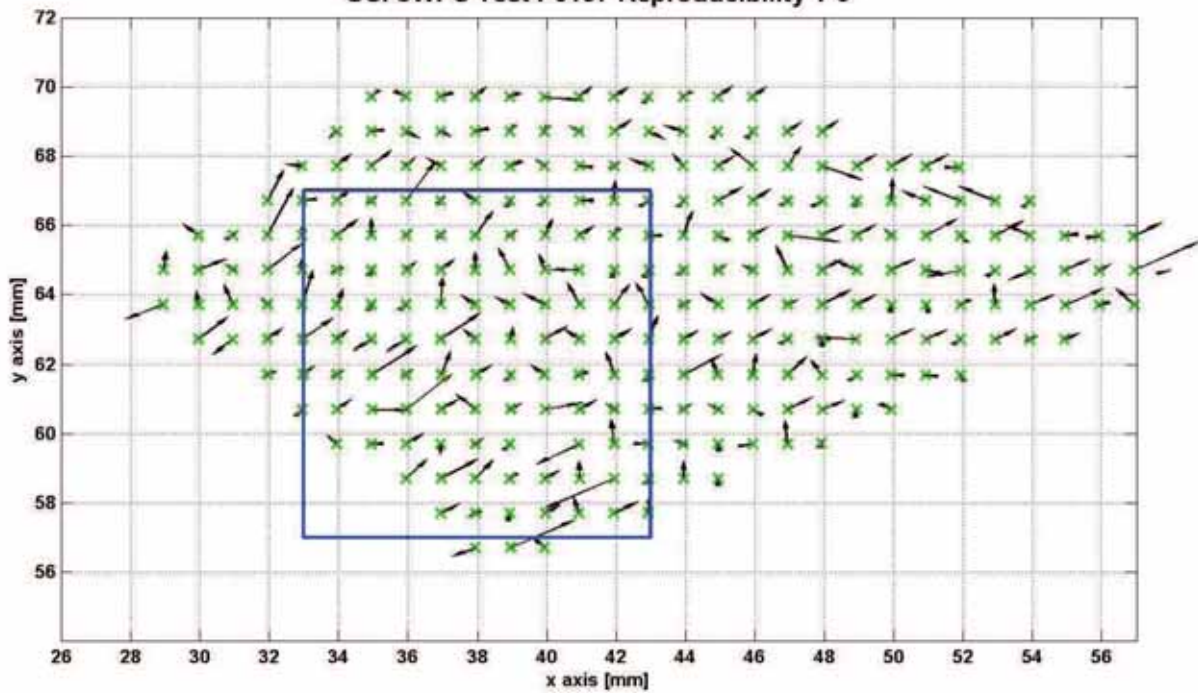
OSI oWPS Test P0201 Reproducibility 1-4



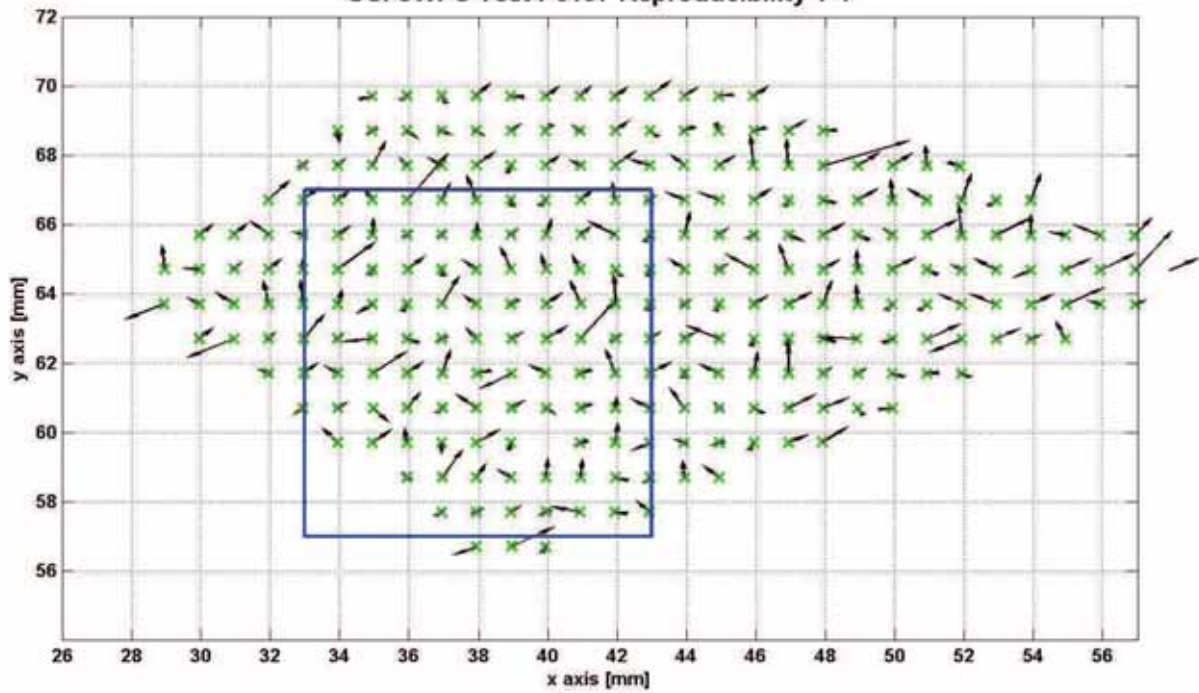
OSI oWPS Test P0197 Reproducibility 1-2



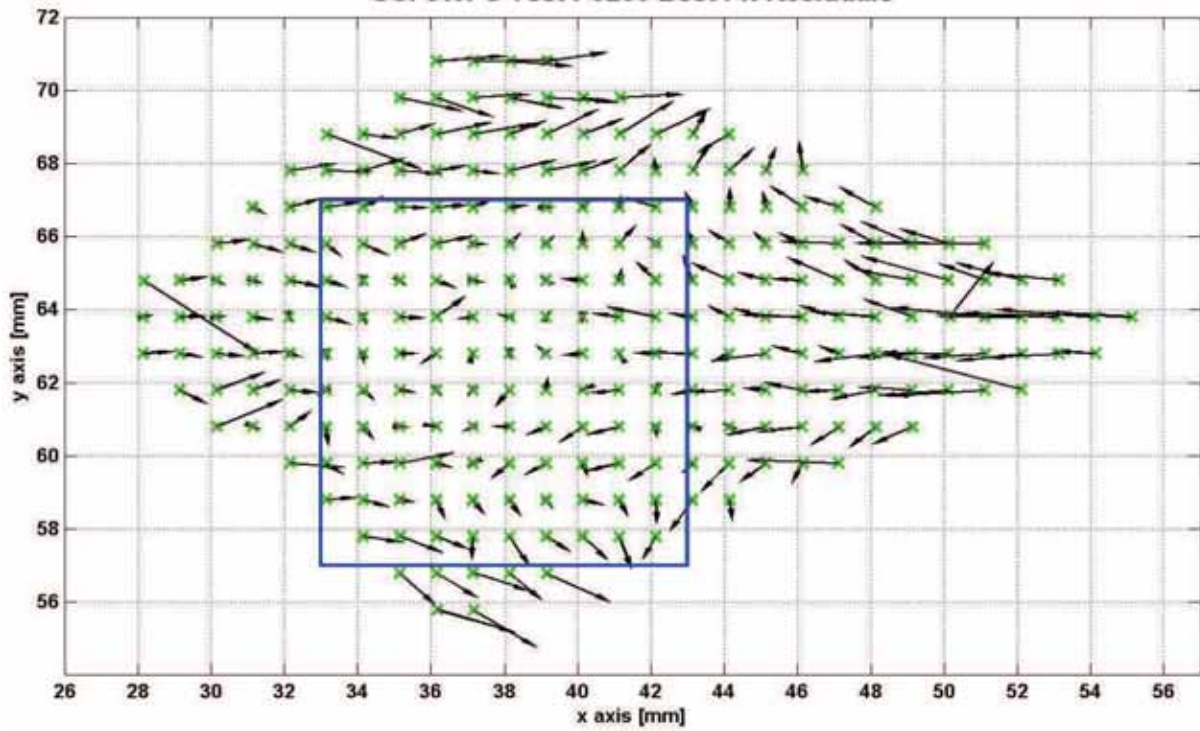
OSI oWPS Test P0197 Reproducibility 1-3

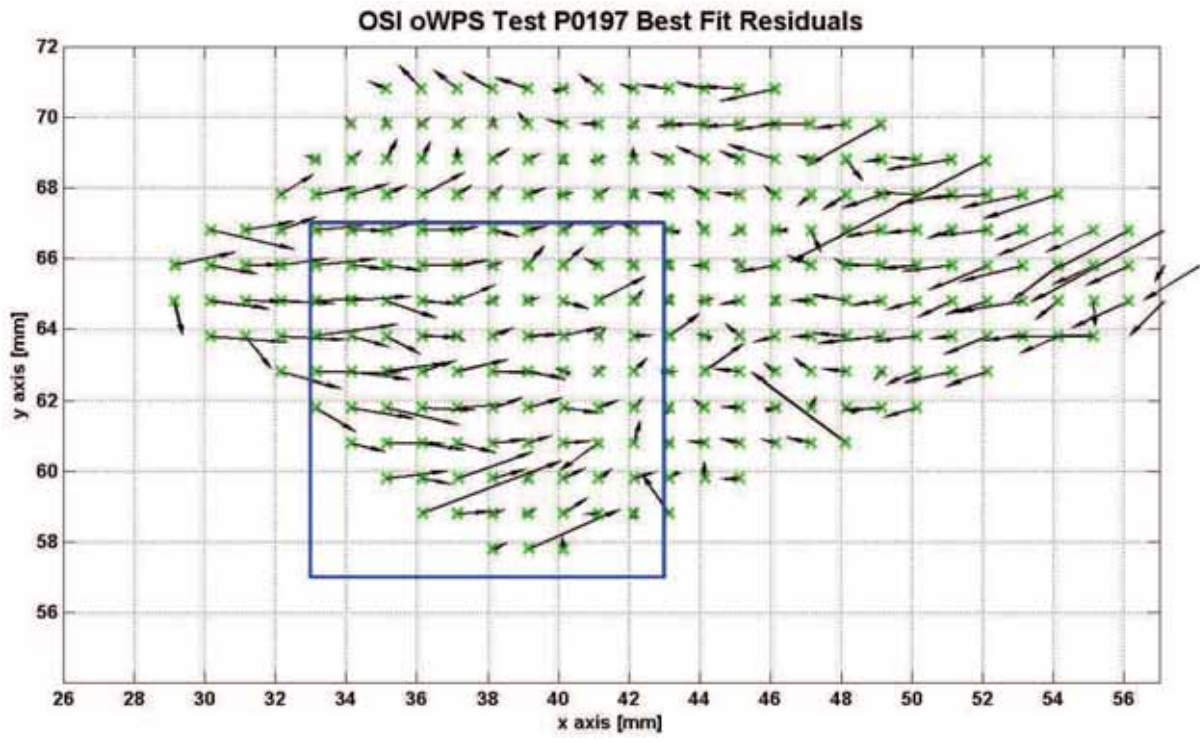
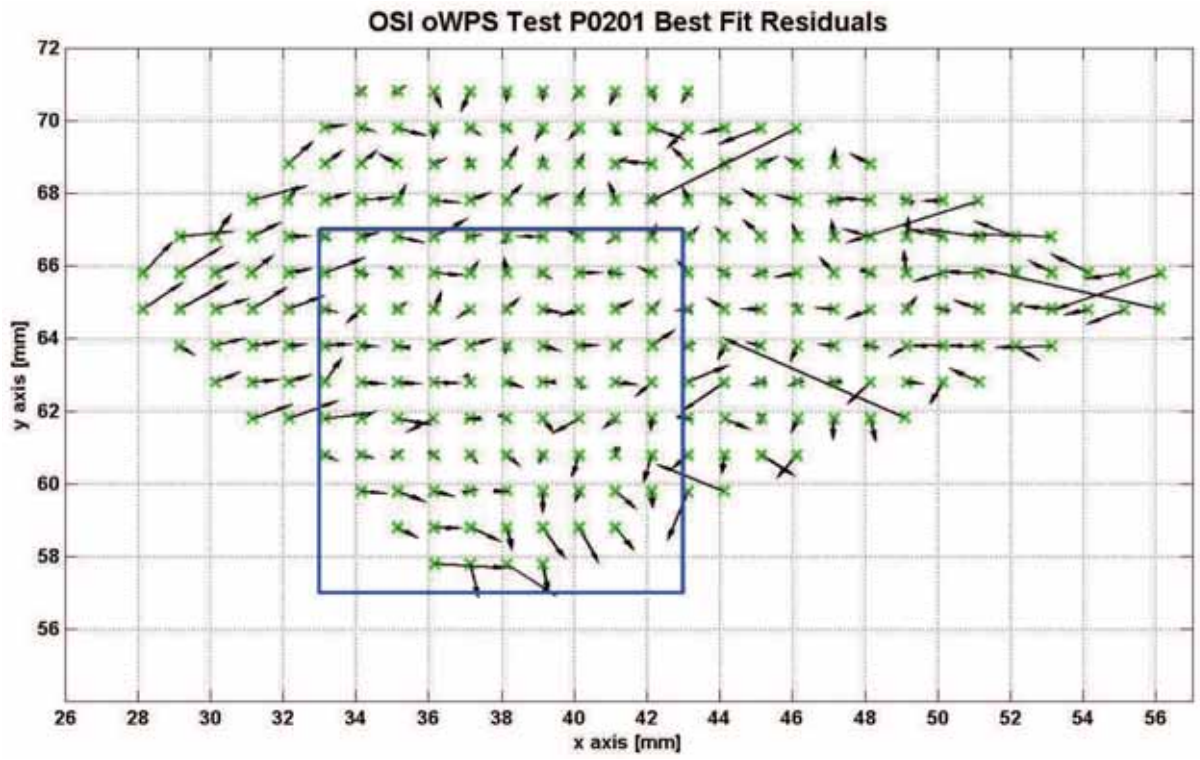


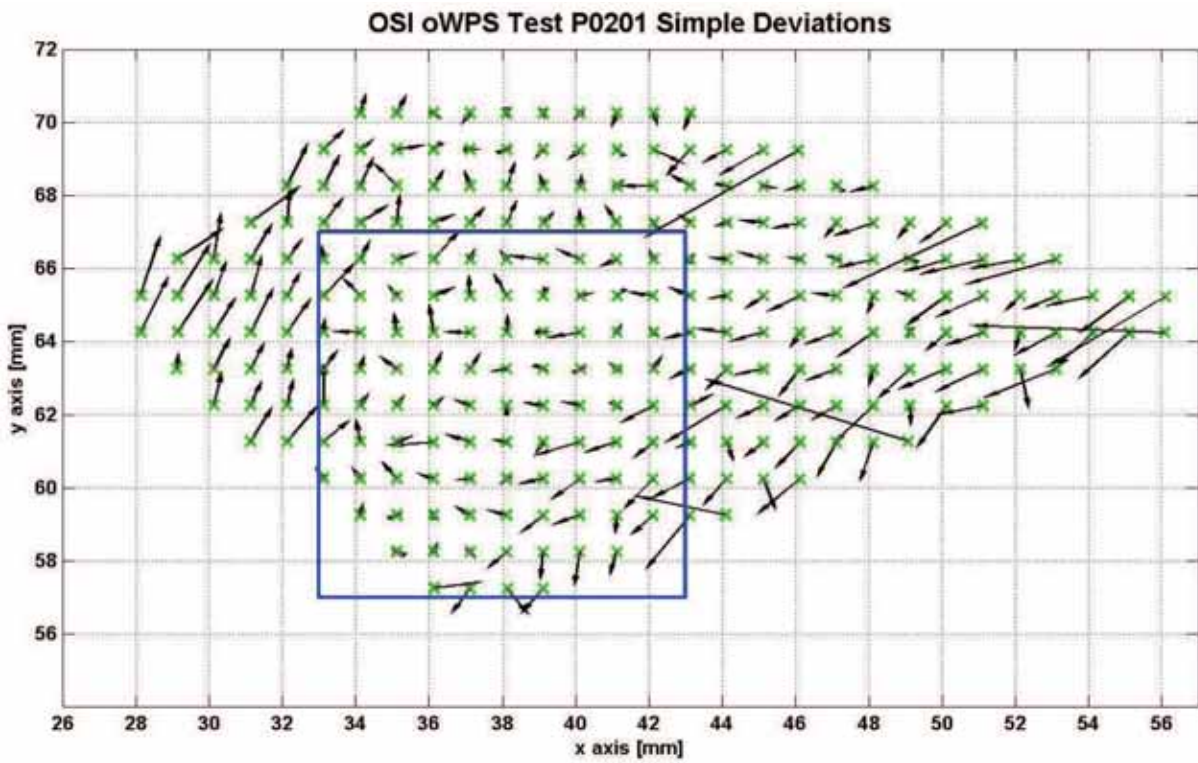
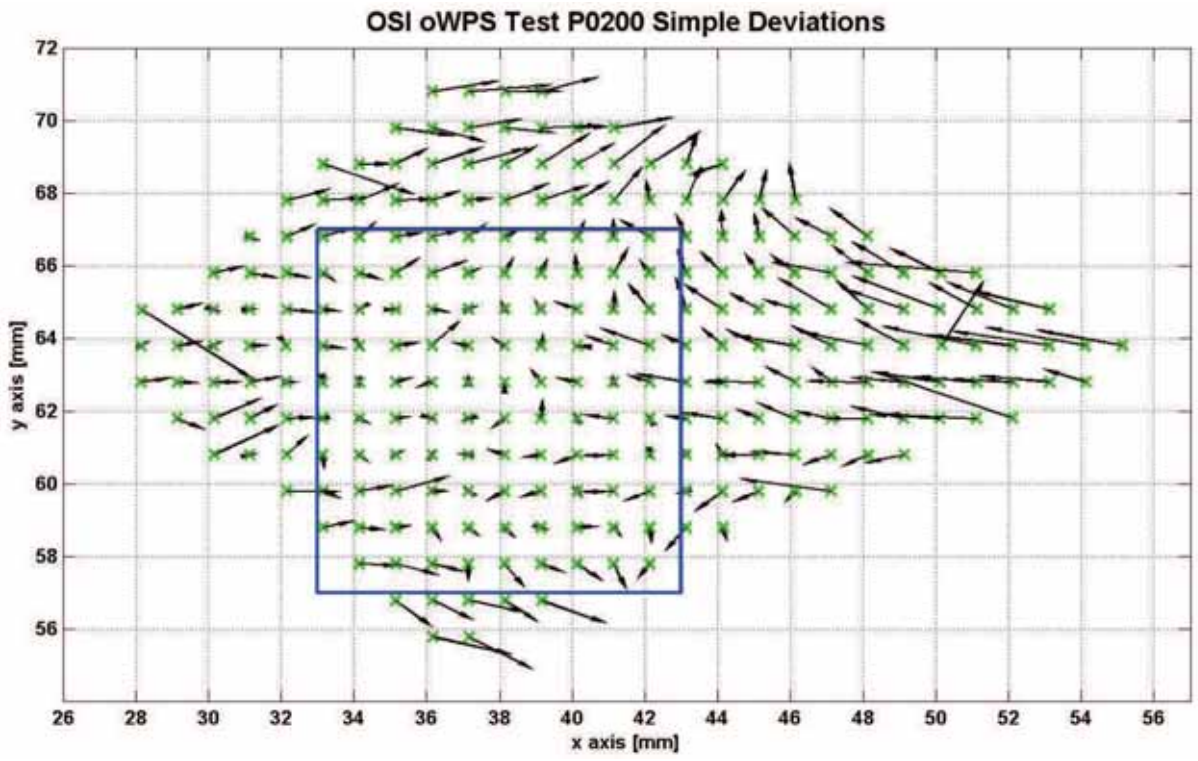
OSI oWPS Test P0197 Reproducibility 1-4



OSI oWPS Test P0200 Best Fit Residuals







OSI oWPS Test P0197 Simple Deviations

